

Coupling the Xinanjiang model to a kinematic flow model based on digital drainage networks for flood forecasting

Jintao Liu,^{1,2} Xi Chen,¹ Jiabao Zhang^{2*} and Markus Flury³

¹ State Key Laboratory of Hydrology-Water Resources and Hydraulic Engineering, Hohai University, Nanjing 210098, People's Republic of China

² State Experimental Station of Agro-Ecosystem in Fengqiu, State Key Laboratory of Soil and Sustainable Agriculture, Institute of Soil Science, Chinese Academy of Sciences, Nanjing 210008, People's Republic of China

³ Department of Crop and Soil Science, Center for Multiphase Environmental Research, Washington State University, Pullman, WA 99164-6420, USA

Abstract:

The Xinanjiang model, which is a conceptual rainfall-runoff model and has been successfully and widely applied in humid and semi-humid regions in China, is coupled by the physically based kinematic wave method based on a digital drainage network. The kinematic wave Xinanjiang model (KWXAJ) uses topography and land use data to simulate runoff and overland flow routing. For the modelling, the catchment is subdivided into numerous hillslopes and consists of a raster grid of flow vectors that define the water flow directions. The Xinanjiang model simulates the runoff yield in each grid cell, and the kinematic wave approach is then applied to a ranked raster network. The grid-based rainfall-runoff model was applied to simulate basin-scale water discharge from an 805-km² catchment of the Huaihe River, China. Rainfall and discharge records were available for the years 1984, 1985, 1987, 1998 and 1999. Eight flood events were used to calibrate the model's parameters and three other flood events were used to validate the grid-based rainfall-runoff model. A Manning's roughness via a linear flood depth relationship was suggested in this paper for improving flood forecasting. The calibration and validation results show that this model works well. A sensitivity analysis was further performed to evaluate the variation of topography (hillslopes) and land use parameters on catchment discharge. Copyright © 2009 John Wiley & Sons, Ltd.

KEY WORDS kinematic wave method; runoff infiltration; drainage network; digital elevation model; land use; Xinanjiang model

Received 5 March 2008; Accepted 8 December 2008

INTRODUCTION

The Xinanjiang model (Zhao, 1992) is a conceptual rainfall-runoff model and has been successfully and widely used in humid, semi-humid and even in dry area of China and elsewhere in the world for flood forecasting since its initial development in the 1970s. The main merit of the Xinanjiang model is that it can account for the spatial distribution of soil moisture storage, which has made it outperform other models in a comparison by Gan *et al.* (1997). The concept of spatial distribution of soil moisture storage has been implemented in other models, e.g. the VIC model (Liang *et al.*, 1996) and the ARNO model (Todini, 1996). Like most conceptual hydrological models with lumped or semi-distributed structure, the spatial variation of hydrological variables is generally difficult to be considered (Chen *et al.*, 2007), which happens to be the advantage of the distributed hydrological models.

In recent decades, owing to their capability of explicit spatial representation of hydrological components and variables, the distributed hydrological models have been increasingly applied to account for spatial variability of

hydrological processes and to support impact assessment studies (e.g. land use change and climate change studies) (Christensen *et al.*, 2007; Das *et al.*, 2008). At the same time, many distributed hydrological models have been developed for storm-runoff simulations, such as the TOPKAPI model (Todini *et al.*, 2001; Liu *et al.*, 2005), LISFLOOD model (De Roo *et al.*, 2000), or the physically based storm-runoff model (Du *et al.*, 2007). Such distributed storm-runoff models do in principle take into account the main mechanisms of flow generation such as saturated-excess overland flow and lateral subsurface flow (Du *et al.*, 2007). Since the data availability was obviously not up to the mark to leverage distributed models, they did not perform better than lumped models (Reed *et al.*, 2004) in the distributed model inter-comparison project (DMIP).

In fact, the model performance can vary depending on many factors such as model structure (distributed or lumped), physiographic characteristics of the basin, data available (resolution/accuracy/quantity), so that no single model is perfect and best for all problems (Du *et al.*, 2007; Das *et al.*, 2008). Though many distributed storm-runoff models, e.g. TOPKAPI model (Liu *et al.*, 2005), Du's model (Du *et al.*, 2007) and LL-II model (Li *et al.*, 2004), have been operationally running for real time flood forecasting purposes, the Xinanjiang model is still one of the most widely used models in humid basins in China due to the lack of spatial data especially soil

* Correspondence to: Jiabao Zhang, State Experimental Station of Agro-Ecosystem in Fengqiu, State Key Laboratory of Soil and Sustainable Agriculture, Institute of Soil Science, Chinese Academy of Sciences, Nanjing 210008, People's Republic of China.
E-mail: jbzhang@mail.issas.ac.cn

data. Therefore, it is necessary and useful to develop a new type of flood forecasting model based on the existing Xinanjiang model to improve the model capability in using more detailed information, such as topography and land cover, in real time flood forecasting. To couple weather radar rainfall data with the Xinanjiang model, the rainfall-runoff model was set to the same resolution ($1 \text{ km} \times 1 \text{ km}$) as the weather radar rainfall (Li *et al.*, 2004). A similar model structure and model resolution ($1 \text{ km} \times 1 \text{ km}$) were used by Lu *et al.* (2008) to couple a mesoscale atmosphere model with the Xinanjiang model. Both of the studies (Li *et al.*, 2004; Lu *et al.*, 2008) aimed to couple rainfall data with higher resolution than traditional rainfall measured by raingage. Thus the Xinanjiang model has been justified for incorporating grid scale resolution as $1 \text{ km} \times 1 \text{ km}$.

Our main objective here is to develop a grid-based Xinanjiang model that can make use of readily available rainfall, land use and topographic data for basin-scale flood forecasting. In this study, a grid-based kinematic wave method is used to couple spatial information into the Xinanjiang model. The coupling is not a virtue in itself, but is a technical way to produce an operational methodology, while reflecting the necessary physical processes. In the model, the basic approximation is that the tension water capacity is spatially heterogeneity and distributed within each grid (such as $1 \text{ km} \times 1 \text{ km}$) like in sub-basin scale. And we also assumed that spatial distribution of tension water capacity is equally the same in every grid, i.e. the curve can be regarded as an accumulative function or statistical description of the spatial heterogeneity for all pixels. Runoff generated on a partial area in each grid is averaged on the whole grid and routed to the downstream grid. The model was tested with a series of rainfall-discharge events from the Huangnizhuang sub-basin of the Huaihe River, China.

ISSUES IN THE FLOW ROUTING MODELS AND A STRATEGY TO MODEL BUILDING

As to the flow routing model used in the conceptual hydrological models, e.g. Xinanjiang model (Zhao, 1992), excess rainfall is usually routed by lumped approaches such as the unit hydrograph, flow isochrones or linear reservoir modelling in computation of overland flow and channel flow. These approaches are conceptually simple and easy to use in flood forecasting, but it is difficult to represent land cover and topography as spatially distributed entities on a basin scale. For many years hydrologists have attempted to relate the hydrologic response of watersheds to its topographic structures. The geomorphologic instantaneous unit hydrograph (GIUH) method (Rodriguez-Iturbe *et al.*, 1979) is perhaps the most promising development in this direction. Maidment and Olivera (1996) proposed a spatially distributed unit hydrograph model in which the watershed is composed of individual cells and the flow paths from cell to cell is determined from the DEM. Ajward and Muzik (2000)

and Zhang *et al.* (2003) also developed such a type of unit hydrograph model based on a GIS. Lohmann *et al.* (1998) derived a linear and time-invariant scheme and runoff was routed from each cell to the river system with without any feedback to the VIC-2L model and without transporting water between neighbouring grids. In these models based on linear systems theory, flow from one cell is not affected by flow from neighbour cells.

The kinematic wave overland flow approach is a physically based method and is well suited for considering both land cover and topography condition. The approach has been frequently used to model the rainfall-runoff process for simple as well as complex watershed geometries (Kibler and Woolhiser, 1970; Singh and Woolhiser, 1976; Michaud and Sorooshian, 1994). It has been used in many distributed hydrological models, e.g. IHDM (Calver *et al.*, 1995), KINEROS (Smith *et al.*, 1995), WEP (Jia *et al.*, 2001) and WEHY (Kavvas *et al.*, 2004). As the grid-square arrangement is adopted by most existed, distributed hydrology model, e.g. SHE (Abbott *et al.*, 1986), TOPKAPI model (Todini *et al.*, 2001; Liu *et al.*, 2005), LISFLOOD model (De Roo *et al.*, 2000), a physically based storm-runoff model (Du *et al.*, 2007), it was used in our model. However, the area of the basic unit termed a sub-basin in the Xinanjiang model is quite larger area than that of the grid-square unit of distributed model. So when applying the physically based kinematic method with the grid-square arrangement into the Xinanjiang model to allow for the easy importation of data from remotely-sensed source, the basin need to be subdivided to modify the Xinanjiang model's structures. The distributed flow routing model is not only capable of accounting for spatial variability of hydrological processes, but it also enables computation of internal fluxes.

THE COMBINED RAINFALL-RUNOFF MODEL AND ITS ADAPTION FOR DIGITAL DRAINAGE NETWORKS

Runoff generation in the kinematic wave Xinanjiang model (KWXAJ)

In the Xinanjiang model (Zhao, 1983, 1992), runoff production at a point occurs on the repletion of storage capacity, i.e. infiltration occurs until the soil moisture capacity is reached. To represent the spatial distribution of the soil moisture storage capacity over the basin, a parabolic curve, i.e. soil moisture storage capacity curve (SMSCC) is used in the Xinanjiang model.

In the modified Xinanjiang model, spatial distribution of rainfall input, vegetation, land use and topographies of the watershed is achieved by a grid network. Here, the grid-based rainfall-runoff model named the kinematic wave Xinanjiang model (KWXAJ) consists of two parts: a runoff yield model and a kinematic overland flow routing model for a grid network. The Xinanjiang model was used to calculate runoff yield in each grid element. The parameters used in the runoff yield component are listed in Table I.

Table I. Parameters used the for runoff yield algorithm in the Xinanjiang model

Parameters	Description	Value
K	Ratio of potential evapotranspiration to pan evaporation	1-25
B	Exponent of the spatial distribution curve of tension water storage capacity	0-3
C	Evapotranspiration coefficient of the deep layer	0-2
IMP (%)	Percentage of the impervious area of catchment	0-01
WUM (mm)	Tension water capacity of the upper layer	20
WLM (mm)	Tension water capacity of the lower layer	60
WDM (mm)	Tension water capacity of the deep layer	40
SM (mm)	Free water storage capacity	15
Ex	Exponent of the spatial distribution curve of free water storage capacity	1-2
Ki	Outflow coefficient of free water storage to the interflow	0-25
Kg	Outflow coefficient of free water storage to the groundwater	0-45

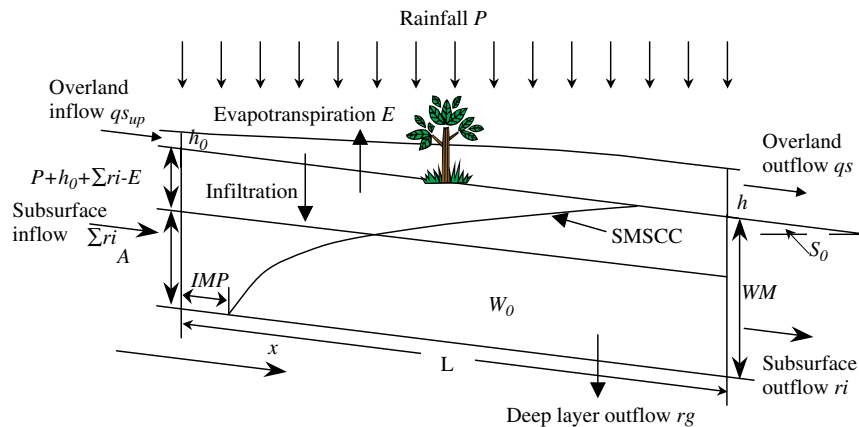


Figure 1. Schematic of runoff generation and the soil moisture storage capacity curve on hillslope for the modified Xinanjiang model (after Zhao, 1992)

Rainfall-runoff processes within each grid of the combined model can be described as follows. When rainfall P exceeds evapotranspiration E , rainfall is infiltrated into soil reservoir and overland flow qs will not occur until the soil reservoir is saturated. Excess water is transferred to downstream grid and finally routed to the outlet. To a given grid, overland flow qs_{up} (the corresponding runoff depth is h_0), subsurface flow ($\sum ri$) from upland grids as well as rainfall are regarded as inflow. So the runoff infiltration, i.e. runoff is considered in the modified Xinanjiang model, which makes it differ from the traditional version of Xinanjiang model. Runoff depth is calculated by the Xinanjiang model and it is separated into overland flow rs , subsurface flow ri , and deep layer flow rg . In Figure 1, the runoff generation on a hillslope with a length L and slope S_0 is shown. The percentage of the impervious area is IMP , W_0 and WM are initial areal mean tension, water storage and areal mean tension water capacity, respectively.

Runoff routing for digital drainage networks

In the kinematic wave model for raster systems, discharge leaving the downstream boundary of a raster enters the upstream boundary of a higher-level raster and serves to establish the boundary conditions of depth and discharge required by the kinematic wave method. Overland flow from any direction to the raster is regarded as lateral inflow. According to the D-8 algorithm (Fairfield

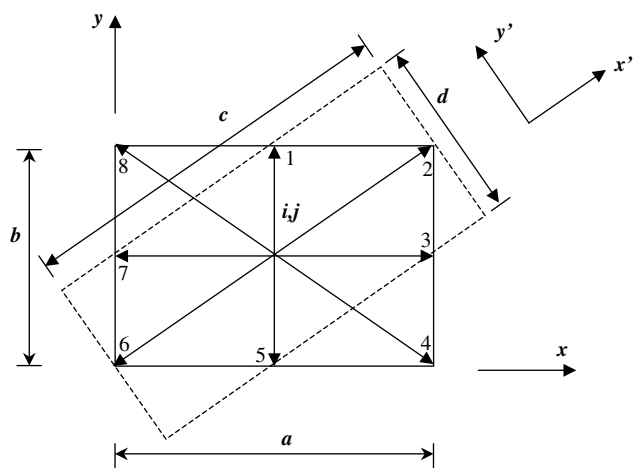


Figure 2. Raster sketch for overland flow routing

and Leymarie, 1991), any raster in the grid system has eight possible flow directions (Figure 2). When the outflow direction is parallel to x or y , the length $L_{i,j}$ of the cell is equal to a and the width $W_{i,j}$ equal to b , when the outflow direction is parallel to the diagonal such as x' , y' , a presumed raster is defined with its length c and width d . The length $L_{i,j}$ and the width $W_{i,j}$ are expressed as:

$$L_{i,j} = \sqrt{a^2 + b^2} \tag{1}$$

$$W_{i,j} = a \cdot b / \sqrt{a^2 + b^2} \tag{2}$$

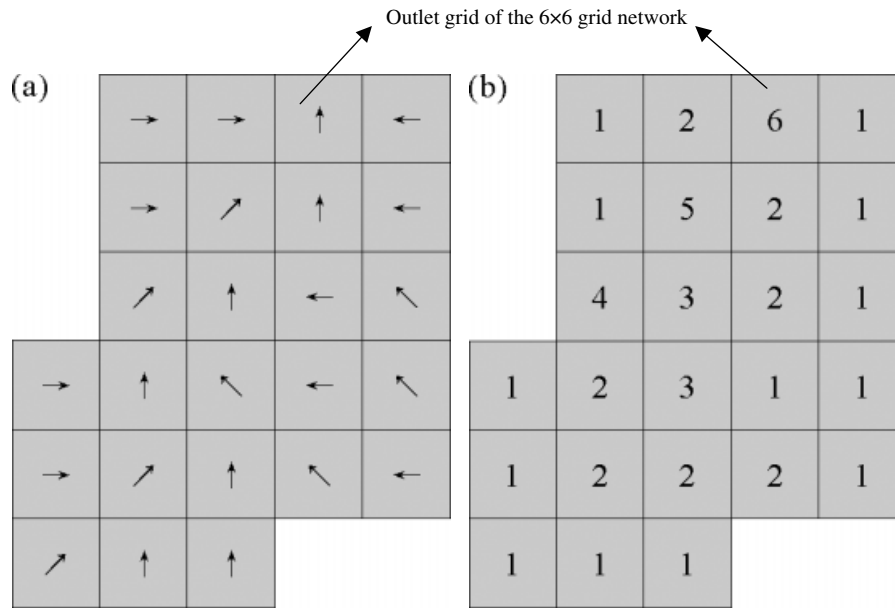


Figure 3. (a) Raster flow direction definition for a 6 × 6 grid network; (b) ranked raster for each raster to the outlet

The drainage network extraction algorithm described by Martz and Garbrecht (1992) was used to implement the structure of the digital drainage network, including the flow vectors and the raster slopes. The flow concentration system of the basin is routed according to a simple algorithm. Each cell has a routing order and the cells are ranked by the following principles: (1) cells without inflow are defined rank 1, and (2) the ranking number of each cell is equal to the maximum ranking number among neighbour upland cells plus 1. There is no flow between cells of equal rank. An example of the flow network and the ranking numbers is shown in Figure 3.

The one-dimensional kinematic wave equation for shallow water flow over is given by:

$$\begin{cases} \frac{\partial h}{\partial t} + \frac{\partial uh}{\partial x} = q_{lat}(x, t) \\ S_0 = S_f \end{cases} \quad (3)$$

Here h is overland flow depth (FD), u is depth average flow velocity, S_0 is the hillslope, $q_{lat}(x, t)$ is the net inflow, and S_f is the friction slope. Under the kinematic wave approximation, the discharge is a function of overland FD (Kibler and Woolhiser, 1970):

$$q = uh = \alpha h^m \quad (4)$$

Here $q(x, t)$ is the flow discharge per unit width, α and m are coefficients. Using Manning's equation, $m = 5/3$ and $\alpha = S_0^{1/2}/n$ in which n is the Manning coefficient (MC). Substitution of Equation 4 into Equation 3 yields the kinematic wave equation with one dependent variable:

$$\frac{\partial h}{\partial t} + \alpha m h^{m-1} \frac{\partial h}{\partial x} = q_{lat}(x, t) \quad (5)$$

An explicit difference method based on the MacCormack scheme (MacCormack, 1971) is employed here to solve the governing differential equations. The resulting difference equations are:

Predictor step:

$$h_i^* = h_i^n - \frac{\Delta t}{\Delta x} (q_{i+1/2}^n - q_{i-1/2}^n) + q_{lat_i}^{n+1/2} \Delta t \quad (6)$$

$$q_{i\pm 1/2}^n = \alpha \left(\frac{h_{i\pm 1}^n + h_i^n}{2} \right)^m \quad (7)$$

Corrector step:

$$h_i^{n+1} = \frac{1}{2} \left[h_i^* + h_i^n - \frac{\Delta t}{\Delta x} (q_{i+1/2}^{n+1/2} - q_{i-1/2}^{n+1/2}) + q_{lat_i}^{n+1/2} \Delta t \right] \quad (8)$$

$$q_{i\pm 1/2}^{n+1/2} = \frac{1}{2} \alpha \left[\left(\frac{h_{i\pm 1}^n + h_i^n}{2} \right)^m + \left(\frac{h_{i\pm 1}^* + h_i^*}{2} \right)^m \right] \quad (9)$$

The initial condition for overland flow is a dry surface

$$h(x, 0) = 0 \quad (10)$$

The boundary condition for cells with their ranking number equal to 1 is taken as zero inflow. Thus,

$$h(0, t) = 0 \quad (11)$$

For other cells, the boundary condition is given below:

$$h(0, t) = \left(\frac{\sum_{k=1}^N q_{sup,k}}{\alpha} \right)^{\frac{1}{m}} \quad (12)$$

where N is the number of upstream inflow cells, $q_{sup,k}$ is the discharge from upstream inflow cell.

Numerical experiments were carried out to compare the performance of the MacCormack schemes with the analytical solution of kinematic wave equations (Singh, 1996) for a hypothetical hillslope. The simulations were applied to a test hillslope of 900 m long and 1 m wide,

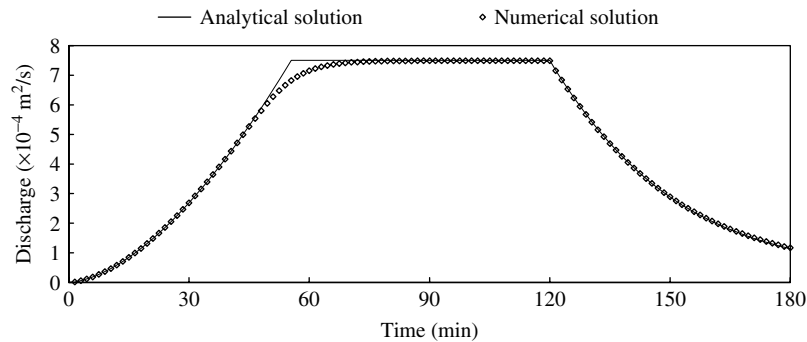


Figure 4. Comparison of numerical experiment results between analytical and numerical solutions

which was subjected to a rainfall of 0.05 mm/min for 120 min. The MC was $n = 0.02$ and the slope of the hillslope was 0.75%. The simulation was run for 300 min using a time step of 90 s and a space discretization of 30 m.

The model performance in terms of discharge was evaluated by the mean absolute error (MAE):

$$MAE = \frac{1}{n} \sum_i^n |q_{in} - q_{ia}| \quad (13)$$

where q_a , q_n represent flow of analytical and numerical solution, respectively. The numerical simulation matched the analytical solution very well, as shown in Figure 4 and confirmed by the low value of $MAE = 4.58 \times 10^{-6} \text{ m}^2/\text{s}$.

Overland flows are routed from the most upstream cells to the outlet cell. Before entering into downstream cells, the subsurface flow of each cell is routed by the 'lag and route' technique used in the original Xinanjiang model. Deep layer outflow (qg) is gathered to the groundwater pool directly (see in Figure 1) and discharge from the groundwater pool is also routed by the 'lag and route' technique.

CASE STUDY AREA AND DATA

We selected the Huangnizhuang basin (Figure 5) for model calibration and validation. This basin has an area of 805 km², and is part of the Shiguanhe basin (31°12' – 32°18'N, 115°17' – 115°55'E) of Huaihe River which has an area of 158 160 km². The Huangnizhuang basin is characterized by mountains and steep slopes. Rainfall is often intense. The annual rainfall is about 1250 mm and the runoff coefficient is about 0.6. Temporal-spatial distribution of the rainfall is uneven and storms are centralized during June to September.

Event hourly discharge and rainfall and daily pan evaporation were monitored at the Huangnizhuang station (31°28'N, 115°37'E). Event hourly rainfall was also monitored at seven other locations in the basin (Figure 5). Hydrological data from 1984, 1985, 1987, 1998 and 1999 were used in this study. The spatial distribution of the precipitation was obtained using Thiessen polygon interpolation (Figure 6a). A DEM for the catchment was available

from the U.S. Geological Survey's EROS Data Center (GTOPO30). Elevations in GTOPO30 are regularly spaced at 30 arcsecond (about 1 km) (Figure 6b). The catchment was discretized in cells of size 30 × 30 inch, and 42 different ranks were assigned (Figure 6c). The frequency distribution of the individual ranks is shown in Figure 7. The higher-order cells correspond to perennial rivers or ephemeral waterways and cells with higher rank than 27 are defined as channel cells by compared with the real channels. We assumed that the MC (n) for channel cells is equal 0.04. Surface slope was derived from DEM data. The slope frequency distribution shows that slopes of about 0.09% were most frequent and the average slope was about 0.122% (Figure 8).

Vegetation distribution of the basin at a spatial resolution of 30 arcsecond was obtained from the UMD 1 km Global Land Cover database for 1999 (<http://www.geog.umd.edu/landcover/1km-map.html>). Six types of vegetation were identified and the distribution is shown in Figure 6d. Nearly 78% of the basin is covered by woodland (Table II). Grids with different vegetation cover (land use) were assumed to have different MCs . The MCs were also different for each storm event as explained below. The soil type is relatively singular in our mountainous Huangnizhuang basin and the soil category is Lithosols according to the FAO Soil Map of the World (FAO, 1998).

RESULTS AND DISCUSSION

Calibration of the model

The Xinanjiang model parameters for Huangnizhuang sub-basin were calibrated by eight flood events. Since most parameters such as K , C , IMP , WUM , WLM , WDM , are related to the average climate and surface conditions of the studied region and as it is one of the tributaries of Shiguanhe basin, they were preset by referring to the existing results by Li *et al.* (2004). Among the parameters of Table I, only B and SM were optimally calibrated as the time and space scale change (Zhao and Liu, 1995). The best selection for ex is between 1.0 and 1.5 and it may be taken as a constant (Zhao and Liu, 1995). Ki and Kg are the outflow coefficients of the free water storage to interflow and groundwater. As the recession during of the upper interflow storage ordinarily lies between 2 and

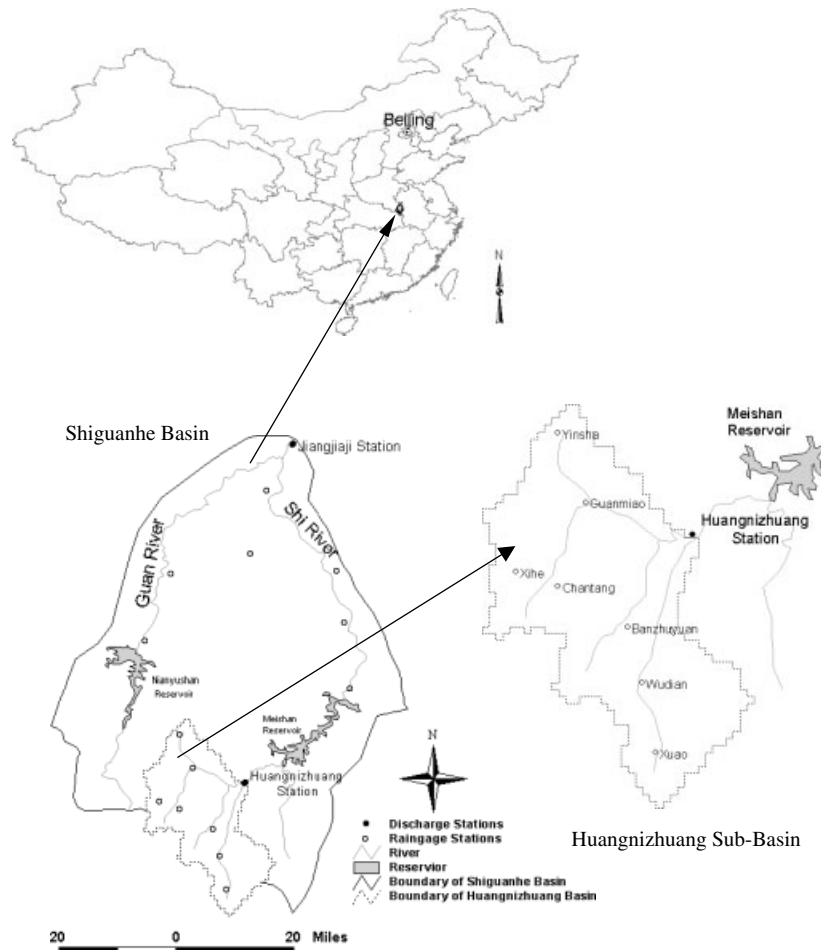


Figure 5. Location of the studied area Huangnizhuang sub-basin in Shiguanhe basin

3 days, it is suggested that the sum $K_i + K_g$ may be taken as 0.7–0.8 and the ratio of the three runoff components will be changed by altering the ratio of K_g/K_i (Zhao and Liu, 1995). Calibration of Manning's roughness is given below in the following text.

The trial and error method was used and we altered the values to make the simulated discharge matching the observed one. In the kinematic wave model, the Manning's roughness coefficients for all of the overland flow cells within the basin were defined according to the land use information and were calibrated for each flood event. The set of MC s used for the flood events are summarized in Table III. The average value of MC s of different flood events varied between 0.082 to 0.194 and for all the flood events selected for calibration the average MC s is 0.116. Those values are comparable to the MC s values obtained from experiments by Woolhiser (1975) and Engman (1986). We generally observed that flood event with large peak flow corresponded to large MC . The average MC was linearly related to the average FD (Figure 9), and the same result was also reported by Wang and Hjelmfelt (1998). This is consistent with the relation for MC s against FD reported by Barling and Moore (1994). In fact, overland flow at very shallow depth encounters maximum resistance because the vegetation is upright in the flow. As pointed by Wang and Hjelmfelt

(1998), the MC here not only depends on the land cover, but also serves as a correction factor for the hydraulic radius approximation. The linear relationship given between the average MC and the average FD shown in Figure 9 indicates that MC is highly related with the flood grade and has great influence on the simulated discharge.

Model performance was evaluated by the efficiency coefficient (EC):

$$EC = 1 - \frac{\sum (Q_{obs} - Q_{sim})^2}{\sum (Q_{obs} - \bar{Q}_{obs})^2} \quad (14)$$

where Q_{obs} and Q_{sim} are observed and simulated discharge (m^3/s), respectively, and \bar{Q}_{obs} is the average value of observed discharge.

The calibration results are summarized in Table IV. Relative errors of the simulated runoff volume range from -17.2 to 0.43% . The peak discharge errors range from 4.2 to 14.0% . By and large, the simulated and observed peak discharges agreed well (Table IV, Figure 10), which is corroborated by an EC value close to 1.

Validation of the model

Three flood events in 1984 and 1987 were selected to validate the performance of the grid-based rainfall-runoff

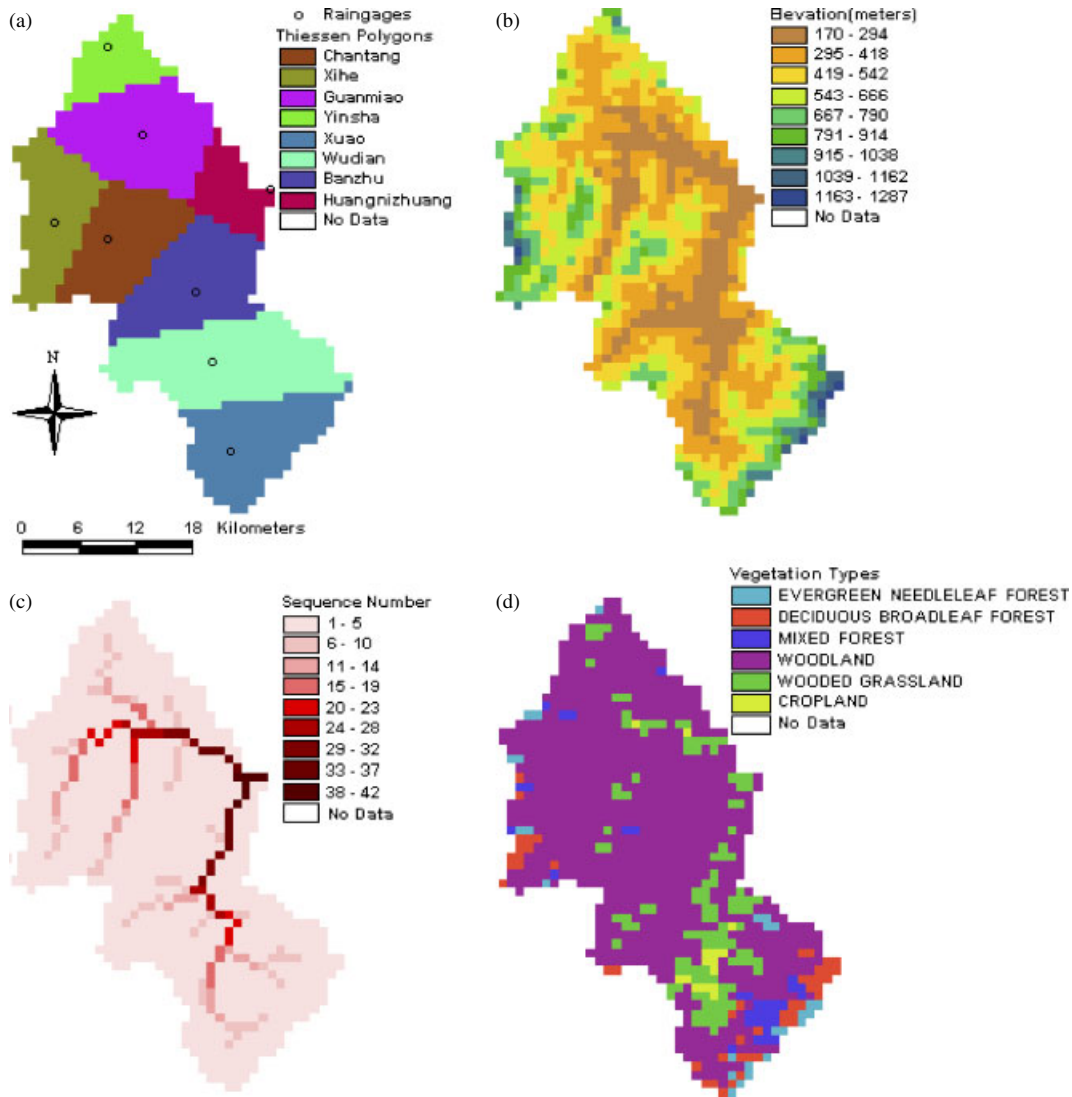


Figure 6. Digital map for Huangnizhaung basin. (a) Thiessen polygons, (b) digital elevation model, (c) sequence number, (d) spatial distribution of vegetation type

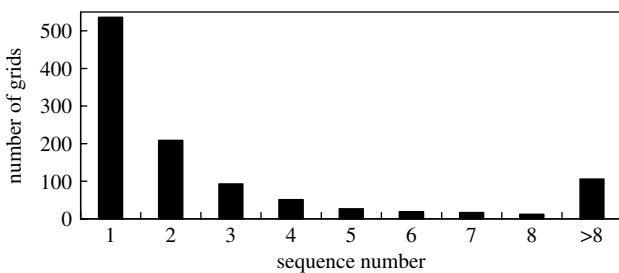


Figure 7. Number of grids of different sequence for kinematic wave routing

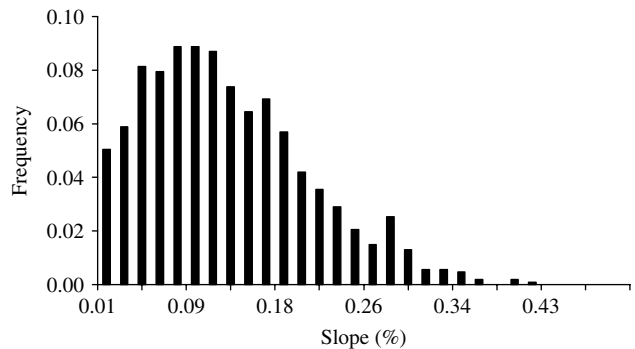


Figure 8. Slope histograms for Huangnizhaung basin

model. Two groups of *MCs* were used for the validation, (1) the average *MCs* shown in Table III and (2) the *MCs* derived from the linear relationship in Figure 9. The simulated results for the three flood events are listed in Table V and in Figure 11. Generally, the observed and simulated hydrographs agree well. The relative errors of runoff volume and peak discharge agree are low, and the *EC* is large (Table V). This indicates that the simulations are consistent with the observations.

Flood event 9, June 1984, was a very small flood compared with flood event 10 and 11. The average *FD* was about 0.54 mm. According to the linear relationship (Figure 9), the *MC* is also relatively small. By using the *MC* derived from the linear relationship, the relative error for the peak discharge was 3.7%, the relative error for the total runoff was -5.3% and *EC* was 0.92 which indicates

Table II. Vegetation types in the Huangnizhuang basin

	Evergreen needle leaf forest	Deciduous broad leaf forest	Mixed forest	Woodland	Wooded grassland	Cropland
Area (km ²)	19.6	36.9	24.8	624.4	88.0	11.3
Percentage (%)	2.4	4.6	3.1	77.6	10.9	1.4

Table III. Manning coefficients for the different flood events

Beginning of flood ^a	Vegetation type						Average value
	Evergreen needleleaf forest	Deciduous broadleaf forest	Mixed forest	Woodland	Wooded grassland	Cropland	
09/09/1984	0.121	0.121	0.165	0.096	0.086	0.077	0.099
05/07/1985	0.135	0.135	0.185	0.107	0.096	0.086	0.110
05/07/1987	0.177	0.177	0.242	0.140	0.126	0.113	0.143
28/08/1987	0.127	0.127	0.173	0.100	0.090	0.081	0.103
02/07/1998	0.110	0.110	0.150	0.090	0.080	0.070	0.092
22/06/1999	0.132	0.132	0.180	0.105	0.094	0.084	0.108
26/06/1999	0.225	0.225	0.310	0.190	0.175	0.150	0.194
29/06/1999	0.102	0.102	0.138	0.080	0.072	0.065	0.082
Average value	0.141	0.141	0.193	0.114	0.102	0.091	0.116

^a Given as dd/mm/yyyy.

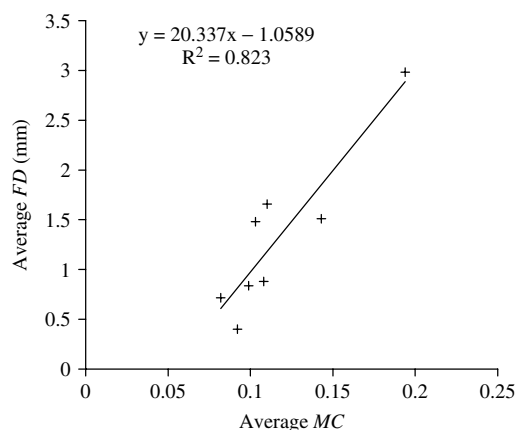


Figure 9. Relationship between the average flow depth and the average *MC*

a good agreement between simulated and observed data. With the average *MC* (Table III), the simulated results were less accurate. There was a 2-h lag between the two simulated peaks as the *MC*s are differed by about 47%.

The average *FD* of Flood event 10, August 1984, was about 0.91 mm and the *MC*s derived from the linear relationship were somewhat smaller than the average value. Using the *MC* derived from the linear relationship and the average *MC*, the relative error for the peak discharge is -6.6, -19.0% and the relative error for the total runoff is 3.3, -4.4% and EC is 0.93, 0.88, respectively. The lag between the two simulated peak discharge was 1 h.

Flood event 11, August 1987, was one of the biggest flood events in this basin. The average *FD* was about 2.54 mm. The *MC*s derived by the linear relationship are larger than the average *MC*s. Again, peak discharge occurred 1 h earlier when using the averaged *MC* as compared to the one derived from the linear relationship.

By and large, the simulations show that the *MC* derived from the linear relationship described the experimental data below better than the average *MC*. Overall, good agreement between model simulations and observed data was observed. All of the simulated results using the average *MC*s and the *MC*s derived from the linear

Table IV. Calibration results by the grid-based rainfall-runoff model for different flood events

No.	Beginning of flood ^a	Observed peak discharge (m ³ /s)	Simulated peak discharge (m ³ /s)	Relative error (%)	Observed runoff volume (×10 ⁴ m ³)	Simulated runoff volume (×10 ⁴ m ³)	Relative error (%)	Efficiency Coefficient
1	09/09/1984	418.0	458.3	9.6	2559.6	2528.4	-1.2	0.91
2	05/07/1985	1100.0	1000.7	-9.0	3506.2	3860.8	10.1	0.90
3	05/07/1987	1127.6	1133.5	0.52	4361.4	4568.9	4.7	0.93
4	28/08/1987	924.6	1054.2	14.0	4398.6	4302.1	-2.2	0.87
5	02/07/1998	213.0	227.0	6.6	1034.8	1016.1	-1.8	0.88
6	22/06/1999	765.0	710.2	-7.2	3172.2	3765.6	18.7	0.89
7	26/06/1999	2150.0	2242.7	4.3	9359.8	9400.3	0.43	0.96
8	29/06/1999	319.0	332.3	4.2	1402.3	1161.2	-17.2	0.71

^a Given as dd/mm/yyyy.

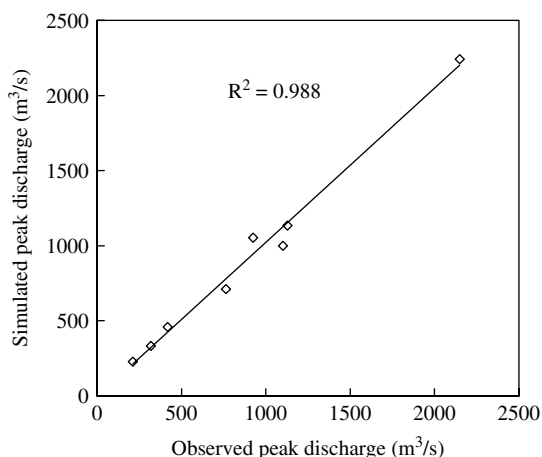


Figure 10. Comparison of observed and simulated peak discharges

relationship reach the accuracy standard according to The Accuracy Standard of Hydrological Forecasting in China (Hydrological Bureau of China, 2000).

Sensitivity analysis

It has been shown in the flood validation simulations that the discharge is greatly influenced by the *MC*. When *MCs* were increased, as in the simulations of Flood 9 and 10, the simulated peak discharge was reduced and peak time deferred. And when *MCs* were decreased as in case of the Flood 11, the simulated peak discharge was enlarged and peak time advanced.

We carried out an uncertainty analysis to evaluate the effects of topography and land use on hydrological water discharge. In the kinematic wave approach, topography and land are represented by the parameter α , i.e., the surface slope (S_0) and the *MC* (n). For the uncertainty analysis, we individually varied surface slope and roughness by ± 5 and $\pm 10\%$ of their original values.

One of the biggest flood events, Flood 7, was used in the uncertainty analysis. The relevant results are shown in Table VI and Figure 12. As the slopes became steeper, the total volume of discharge as well as the peak discharge increased. Correspondingly, as *MCs* increased, both total discharge and peak discharge decreased. Moreover, when roughness was increased by 10% the peak discharge occurred 1 h later and when it was decreased

by 10% the peak discharge occurred 1 h earlier than the observed one as shown in Table VI and Figure 12.

We calculate the relative variation of total runoff and peak discharge as a function of slope and Manning roughness. The total runoff varied from -2.24 to 1.92% and peak discharge varied from -3.72 to 2.09% when surface slope changed by $\pm 10\%$ (Figure 13). When Manning roughness was changed by $\pm 10\%$, the total runoff varied from 4.11 to -4.23% and peak discharge from 5.88 to -6.55% (Figure 13). These results show that Manning roughness is the more sensitive parameter than the slope, and that the peak discharge is more sensitive than the total runoff.

From this uncertainty analysis, it was clear that surface slope and Manning roughness are two most important characteristics that determine the overland flow routing. One deduction may be that if a large area of the catchment was reclaimed as crop land or as urban development, for both of which the surface roughness is low, the runoff volume will increase as will the peak discharge. Even worse, the peak time of the discharge will be advanced. This can ultimately lead to enhanced soil erosion by more intensive overland flow and flooding.

SUMMARY AND CONCLUSIONS

A modified Xinanjiang model was developed for basin-scale flood modelling. The KWXAJ works on a raster system for representing the spatial heterogeneity of the basin and can fully utilize distributed information of model's inputs, such as rainfall from weather radar, topography and land uses. The Xinanjiang model was used for grid runoff yield in the rainfall-runoff model. The kinematic wave method was used as overland flow routing model for the grid-based rainfall-runoff model in this paper. And before determining runoff depth for a cell using Xinanjiang model, inflow from upstream cells, i.e. the runoff infiltration, was considered.

The main objective of this paper has been to demonstrate the practical implementation of a basin-scale rainfall-runoff model coupled by a distributed flow routing model for flood forecasting and its ability to simulate a variety of basin responses. The simulations match

Table V. Validation results by the grid-based rainfall-runoff model for different flood events

No.	Beginning of flood ^a	Observed peak discharge (m ³ /s)	Simulated peak discharge (m ³ /s)	Relative error (%)	Observed runoff volume ($\times 10^4$ m ³)	Simulated runoff volume ($\times 10^4$ m ³)	Relative error (%)	Efficiency coefficient
Manning coefficients are derived by the linear relationship between the average <i>FD</i> and the average <i>MC</i>								
9	08/08/1984	718.0	670.4	-6.6	1821.2	1882.2	3.3	0.93
10	12/06/1984	164.3	170.3	3.7	985.1	933.3	-5.3	0.92
11	22/08/1987	1928.2	1617.5	-16.1	5660.1	6571.5	16.1	0.92
Manning coefficients are derived by the average value in Table III								
9	08/08/1984	718.0	581.5	-19.0	1821.2	1740.7	-4.4	0.88
10	12/06/1984	164.3	132.1	-19.7	985.1	837.7	-15.0	0.79
11	22/08/1987	1928.2	1912.3	-0.82	5660.1	6699.9	18.4	0.86

^a Given as dd/mm/yyyy.

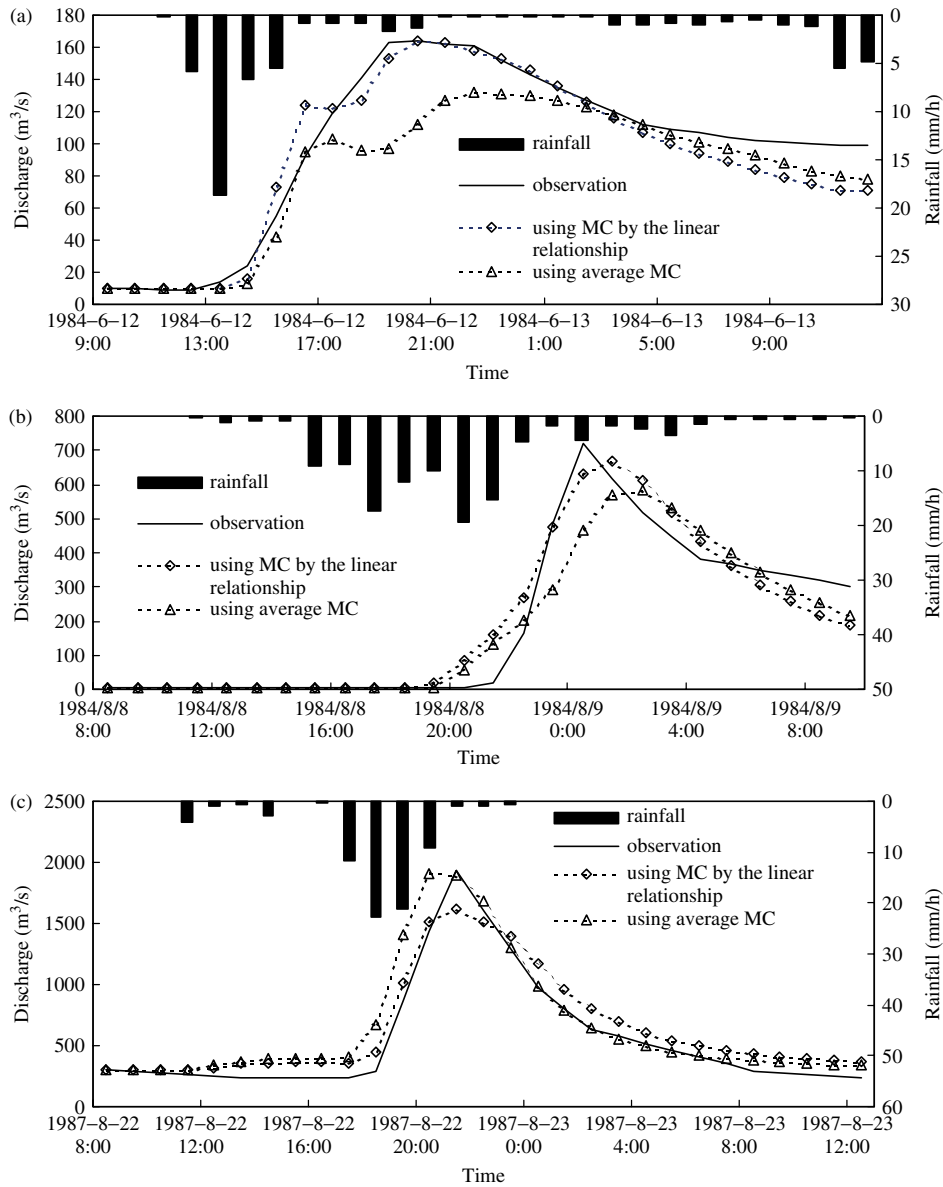


Figure 11. Observed and simulated hydrograph for three flood events in the Huangnizhuang station. (a) Flood event 9, (b) Flood event 10, (c) Flood event 11

Table VI. Simulation results under different topography and land use

Different topography and land use ^a	Total runoff volume ($\times 10^4$ m ³)	Relative error (%)	Peak discharge (m ³ /s)	Relative error (%)	Peak time error (h) ^b	Efficiency coefficient
Observation	9359.8		2150			
SLOP90	9189.3	1.8	2159.3	-0.4	0	0.95
SLOP95	9297.9	0.66	2206.1	-2.6	0	0.95
SLOP105	9494.1	-1.4	2270.1	-5.6	0	0.96
SLOP110	9582.6	-2.39	2290.1	-6.5	0	0.96
ROUGH90	9794.4	-4.7	2377.3	-10.6	1	0.96
ROUGH95	9596.3	-2.5	2292.7	-6.6	0	0.96
ROUGH105	9204.4	1.7	2166.5	-0.77	0	0.96
ROUGH110	9011.3	3.7	2100.9	1.8	-1	0.94

^a SLOP90, SLOP95, SLOP105, SLOP110 represent slopes equal to original slope being multiplied by 0.90, 0.95, 1.05, 1.10, respectively, while the value of the roughness are not changed. ROUGH90, ROUGH95, ROUGH105 and ROUGH110 have the same meaning for the Manning coefficients as explained for the slope.

^b '0' means the simulated peak time equals to the observed peak time, '1' means the simulated peak time is 1 h ahead of the observed peak time, '-1' means the simulated peak time is 1 h behind of the observed peak time.

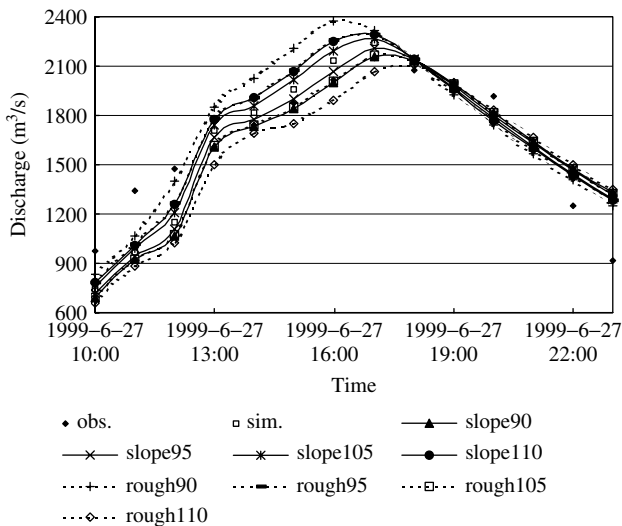


Figure 12. Simulated hydrograph of Huangnizhuang station by changing slope and Manning coefficients

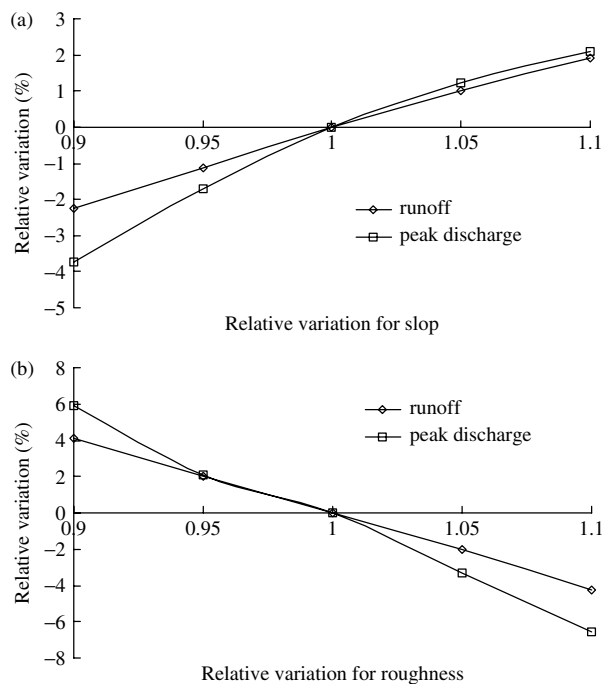


Figure 13. Total runoff and peak discharge variation (%) versus variation of surface slope (a) and roughness (b)

the observations closely. The calibration and validation results show that MC is highly related with the flood grade and large flood events have larger values of MC s whereas small events have smaller values. A relationship between MC and FD is derived in this paper. A sensitivity analysis was used to reveal the performance of this model. The effects of topography and land use were assessed in a series of numerical simulations. The analysis showed that both of surface slope and land use considerably affect total predicted runoff volume and peak discharge. The sensitivity analysis indicates that changes in land use, such as changing forest land to crop or urban land or town, have the potential to increase peak flow and advance the peak time.

Although the grid-based model has been verified in flood event modelling, we realize that soil and other land surface conditions are strong heterogenous, even in a $1 \times 1 \text{ km}^2$ pixel. In this case, pixel parameters from the several groups or a singular set can not be fully accumulated or integrated into the spatial distribution curve of the Xinanjiang model (XM). This is what we believe the limitation of the present grid-based hydrological models. Even though these models' structure in description of spatial distribution is physically reasonable, their applications in watershed hydrological simulation still exist uncertainties due to difficulty in parameter determination for each grid. Adopting the tension water capacity curve of XM in our model development can be regarded as a compromise between physical reasonability and application feasibility for the grid-based hydrological modelling. So when using the Xinanjiang model with small grid scales ($1 \text{ km} \times 1 \text{ km}$), many questions are still to be answered. For instance (1) What is the spatial distribution of the tension water capacity within each grid? (2) How can the tension water capacity be estimated from vegetation and soil texture data? (3) How should we route runoff generated in partial area of the grids?

ACKNOWLEDGEMENTS

This work was supported by the Innovation program of Chinese Academy of Sciences (kzcx2-yw-406), the National Basic Research Program of China (973 project: 2005CB121103), the Key Research Grant from Chinese Ministry of Education (Project No. 308012) and the National Natural Science Foundation of China (Grant No.: 40801013).

REFERENCES

- Abbott MB, Bathurst JC, Cunge JA, O'Connell PE. 1986. An introduction to the European Hydrological System-Système Hydrologique Européen, "SHE", 2, Structure of a physically-based, distributed modeling system. *Journal of Hydrology* **87**: 61–77.
- Ajward MH, Muzik I. 2000. A Spatially Varied Unit Hydrograph Model. *Journal of Environmental Hydrology* **8**: 1–8.
- Barling RD, Moore ID. 1994. Role of buffer strips in management of waterway pollution: a review. *Environmental Management* **18**: 543–558.
- Calver A, Wood WL. 1995. The institute of hydrology distributed model. In *Computer Models of Watershed Hydrology*, Singh VP (ed.). Water Resource publications: Colorado; 595–626, Chapter 17.
- Chen X, Chen YD, Xu CY. 2007. A distributed monthly hydrological model for integrating spatial variations of basin topography and rainfall. *Hydrological Processes* **21**: 242–252.
- Christensen N, Lettenmaier DP. 2007. A multimodel ensemble approach to assessment of climate change impacts on the hydrology and water resources of the Colorado River basin. *Hydrology and Earth System Sciences* **11**: 1417–1434.
- Das T, Bárdossy A, Zehe E, He E. 2008. Comparison of conceptual model performance using different representations of spatial variability. *Journal of Hydrology* **356**: 106–118.
- De Roo APJ, Wesseling CG, Van Deursen WPA. 2000. Physically-based river basin modelling within a GIS: The LISFLOOD model. *Hydrological Processes* **14**: 1981–1992.
- Du JK, Xie SP, Xu YP, Xu CY, Singh VP. 2007. Development and testing of a simple physically-based distributed rainfall-runoff model for storm runoff simulation in humid forested basins. *Journal of Hydrology* **336**: 334–346.

- Engman ET. 1986. Roughness coefficients for routing surface runoff. *Journal of Irrigation and Drainage Engineering-ASCE* **112**(1): 39–53.
- Fairfield J, Leymarie P. 1991. Drainage networks from grid digital elevation models. *Water Resources Research* **27**: 709–717.
- FAO. 1998. Land and water digital media series N-1, December, ISBN 92-5-104050-8.
- Gan TF, Dlamini EM, Biftu GF. 1997. Effects of model complexity and structure, data quality, and objective functions on hydrologic modeling. *Journal of Hydrology* **192**: 81–103.
- Jia YW, Ni GS, Kawahara Y, Suetsugi T. 2001. Development of WEP model and its application to an urban watershed. *Hydrological Processes* **15**: 2175–2194.
- Kavvas ML, Chen ZQ, Dogrul C, Yoon JY, Ohara N, Liang L, Aksoy H, Anderson ML, Yoshitani J, Fukami K, Matsuura T. 2004. Watershed environmental hydrology (WEHY) model based on upscaled conservation equations: hydrologic module. *Journal of Hydraulic Engineering-ASCE* **9**: 450–464.
- Kibler DF, Woolhiser DA. 1970. Mathematical properties of the kinematic cascade. *Journal of Hydrology* **15**: 131–147.
- Li ZJ, Ge WZ, Liu JT, Zhao K. 2004a. Coupling between weather radar rainfall data and a distributed hydrological model for real-time flood forecasting. *Hydrological Sciences Journal-Journal Des Sciences Hydrologiques* **49**: 945–958.
- Li L, Zhu RR, Zhong MJ. 2004b. Application of LL-II distributed rainfall-runoff model based on GIS. *Water Resources Power* **22**(1): 8–11, (in Chinese).
- Liang X, Lettenmaier DP, Wood EF. 1996. One-dimensional statistical dynamic representation of subgrid spatial variability of precipitation in the two-layer variable infiltration capacity model. *Journal of Geophysical Research* **101**(D16): 21: 403–21, 422.
- Liu Z, Martina MVL, Todini E. 2005. Flood forecasting using a fully distributed model: application of the TOPKAPI model to the Upper Xixian Catchment. *Hydrology and Earth System Sciences* **9**: 347–364.
- Lohmann D, Raschke E, Nijssen B, Lettenmaier DP. 1998. Regional scale hydrology: I. Formulation of the VIC-2L model coupled to a routing model. *Hydrological Sciences Journal-Journal des Sciences Hydrologiques* **43**: 131–141.
- Lu GH, Wu ZY, Wen L, Lin CA, Zhang JY, Yang Y. 2008. Real-time flood forecast and flood alert map over the Huaihe River Basin in China using a coupled hydro-meteorological modeling system. *Science in China Series E-Technological Sciences* **51**: 1049–1063.
- MacCormack RW. 1971. Numerical solution of the interaction of a shock wave with a laminar boundary layer. *Lecture Notes in Physics* **8**: 151–163, Springer-Verlag.
- Maidment DR, Olivera F. 1996. Unit Hydrograph Derived From A Spatially Distributed Velocity Field. *Hydrological Processes* **10**: 831–844.
- Martz LW, Garbrecht J. 1992. Numerical definition of drainage network and subcatchment areas from digital elevation models. *Computers & Geosciences* **18**: 747–761.
- Michaud JD, Sorooshian S. 1994. Comparison of simple versus complex distributed runoff models on a mid-sized, semiarid watershed. *Water Resources Research* **30**: 596–605.
- Reed S, Koren V, Smith M, Zhang Z, Moreda F, Seo DJ, DMIP Participants. 2004. Overall distributed model intercomparison project results. *Journal of Hydrology* **298**: 27–60.
- Rodriguez-Iturbe I, Valdes JB. 1979. The geomorphologic structure of hydrologic response. *Water Resources Research* **15**: 1409–1420.
- Singh VP. 1996. *Kinematic Wave Modeling in Water Resources: Surface Water Hydrology*. John Wiley and Sons: New York.
- Singh VP, Woolhiser DA. 1976. A nonlinear kinematic wave model for watershed surface runoff. *Journal of Hydrology* **31**: 221–243.
- Smith ER, Goodrich DC, Woolhiser DA, Unkrich CL. 1995. KINEROS-A kinematic runoff and erosion model. In *Computer Models of Watershed Hydrology*, Chapter 7, Singh VP (Ed.). Water Resources Publication: Colorado: 697–732.
- Todini E. 1996. The ARNO rainfall-runoff model. *Journal of Hydrology* **175**: 339–382.
- Todini E, Ciarapica L. 2001. The TOPKAPI model. In *Mathematical models of large watershed hydrology*, Chapter 12, Singh VP (Ed.). Water Resources Publications: Colorado, USA.
- Wang MH, Hjelmfelt AT. 1998. DEM based overland flow routing model. *Journal of Hydraulic Engineering-ASCE* **3**: 1–8.
- Woolhiser DA. 1975. Simulation of unsteady overland flow. In *Unsteady Flow in Open Channels*, Vol. II Mahmood K, Yevjevich V (eds). Water Resources Publications: Fort Collins, Co; 502.
- Zhang Q, Tan LY, Xu YP, Ge XP. 2003. Exploration of distributed unit hydrograph mode to rainfall-runoff. *Journal of Nanjing University* **39**: 139–143, (in Chinese).
- Zhao RJ. 1983. *Watershed Hydrological Model—Xinjiang Model and Shanbei Model*. Water & Power Press: Beijing, (in Chinese).
- Zhao RJ. 1992. The Xinjiang model applied in China. *Journal of Hydrology* **135**: 371–381.
- Zhao RJ, Liu XR. 1995. The Xinjiang model. In *Computer Models of Watershed Hydrology*, Singh VP (ed.). Water Resources Publication: Colorado; 215–232, Chapter 7.